# Single-Molecule Characterization of DNA–Protein Interactions Using Nanopore Biosensors

**A.H. Squires*, T. Gilboa†, C. Torfstein†, N. Varongchayakul‡, A. Meller†,‡,1**

*Stanford University, Stanford, CA, United States
†The Technion, Haifa, Israel
‡Boston University, Boston, MA, United States
1Corresponding author: e-mail address: ameller@technion.ac.il

## Contents



## Abstract

Detection and characterization of nucleic acid–protein interactions, particularly those involving DNA and proteins such as transcription factors, enzymes, and DNA packaging proteins, remain significant barriers to our understanding of genetic regulation. Nanopores are an extremely sensitive and versatile sensing platform for label-free detection of single biomolecules. Analyte molecules are drawn to and through a nanoscale aperture by an electrophoretic force, which acts upon their native charge while in the sensing region of the pore. When the nanopore's diameter is only slightly larger than the biopolymer's cross section (typically a few nm); the latter must translocate through the pore in a linear fashion due to the constricted geometry in this region. These features allow nanopores to interrogate protein–nucleic acids in multiple sensing modes: first, by scanning and mapping the locations of binding sites along an analyte molecule, and second, by probing the strength of the bond between a protein and nucleic acid, using the native charge of the nucleic acid to apply an electrophoretic force to the complex while the protein is geometrically prevented from passing through the nanopore. In this chapter, we describe progress toward nanopore sensing of protein–nucleic acid complexes in the context of both mapping binding sites and performing force

*Methods in Enzymology*
ISSN 0076-6879
http://dx.doi.org/10.1016/bs.mie.2016.08.010

spectroscopy to determine the strength of interactions. We conclude by reviewing the strengths and challenges of the nanopore technique in the context of studying DNA–protein interactions.

## 1. INTRODUCTION

The ability to sense and characterize individual biomolecules has transformed biological and biomedical research. Substituting ensemble-averaged bulk observations with direct, real-time analysis of single molecules and biomolecular complexes has not only enabled scientists to *critically and quantitatively assess* commonly accepted models that describe biomolecular function, but has also extended the ability to characterize biomolecules and cells at unprecedented temporal and spatial resolutions. To that end, many sophisticated single-molecule (sm) techniques have been evolved by the scientific community. Examples include single ion channel sensing, atomic force microscopy, optical and magnetic tweezers, sm-fluorescence, sm-fluorescence resonance energy transfer, and superresolution microscopy, among others. These techniques offer diverse capabilities for the life sciences, biophysics, and bioengineering, from precision application of small forces on single molecules while measuring their response, to real-time measurements of inter- and intramolecular nanoscale distances, to imaging fine details at the molecular scale using superresolution techniques.

Nanopore sensing is one of the latest additions to the growing arsenal of sm-methods (Wanunu & Meller, 2008). This method is based on two general principles: first, biomolecules are electrokinetically funneled to a spatially localized volume where sensing takes place (Meller & Branton, 2002). This process typically involves electrophoretic forces, which can draw electrically charged individual DNAs or proteins to the sensing region from far away, allowing efficient sampling of the molecules in a given specimen (Wanunu, Morrison, Rabin, Grosberg, & Meller, 2010). Second, the sensing volume consists of an electrically biased water-filled aperture that is only a few nanometers wide—suitable for probing individual molecules. As the molecules are electrokinetically pulled through the aperture, the changes in its ionic conductance are recorded, providing a real-time signature of the passing molecule (Akeson, Branton, Kasianowicz, Brandin, & Deamer, 1999; Kasianowicz, Brandin, Branton, & Deamer, 1996; Meller, Nivon, Brandin, Golovchenko, & Branton, 2000; Meller, Nivon, & Branton, 2001). Both the funneling and sensing processes rely on the intrinsic

biomolecular properties of the analyte molecule (i.e., its electrical charge). Therefore, nanopore sensing does not require tagging or chemical modification of the biomolecules, making it one of the few label-free sm-techniques available.

Another important feature of the nanopore technique lies in its ability to linearize long biopolymer coils during their detection. For example, consider a long biopolymer (e.g., DNA or RNA) with chain cross section $a$, and a nanopore of diameter $d$, where $d$ is only slightly larger than $a$ and is much smaller than the polymer's coil size. When this biopolymer is threaded through the nanopore, the polymer coil structure must be deformed and linearized by the narrow constriction (Fig. 1A). Thus, the ionic conductance of the partially blocked nanopore can be directly related to the local cross section, structure, or other chemical properties of the linearized biopolymer (Wanunu, Sutin, McNally, Chow, & Meller, 2008; Wanunu, Sutin, & Meller, 2009). This powerful feature of the nanopore method can be utilized for scanning and sensing local changes along the length of the biopolymers.

To date, most efforts have been invested in using this scanning principle for the development of ultrafast sm-DNA sequencing approaches (Bayley, 2015; Branton et al., 2008). Specifically, protein-based nanopores such as the *Mycobacterium smegmatis* porin channel are utilized in single-stranded DNA (ssDNA) sequencing where the DNA strand is fed through the nanopore in a base-by-base sequential manner while the ion current provides an electrical signature dictated by the roughly 3–4 nucleotides residing at the smallest constriction of the pore during each step (Cherf et al., 2012; Manrao et al., 2012). This approach has gained substantial interest in part due to its inherent ability to process extremely long biopolymers (thousands of nucleotides) quickly, potentially offering the ability for ultra-long read DNA sequencing. Other emerging and related applications of nanopore biosensing include high-resolution observations of DNA or RNA enzyme motor dynamics by probing the modulations in the ion current flowing through the pore during their activity (Derrington et al., 2015). This class of nanopore biosensing applications is the subject of a review "Subangstrom measurements of enzyme function using a biological nanopore, SPRNT" by Laszlo et al. included in this volume.

A closely related emerging application of nanopore sensing is protein sequencing. Similar to the nucleic acid sequencing approaches described earlier, nanopores can be used to sequence proteins either by denaturing or mechanically unfolding the biomolecules (Oukhaled et al., 2011; Pastoriza-Gallego et al., 2011; Payet et al., 2012; Rodriguez-Larrea &

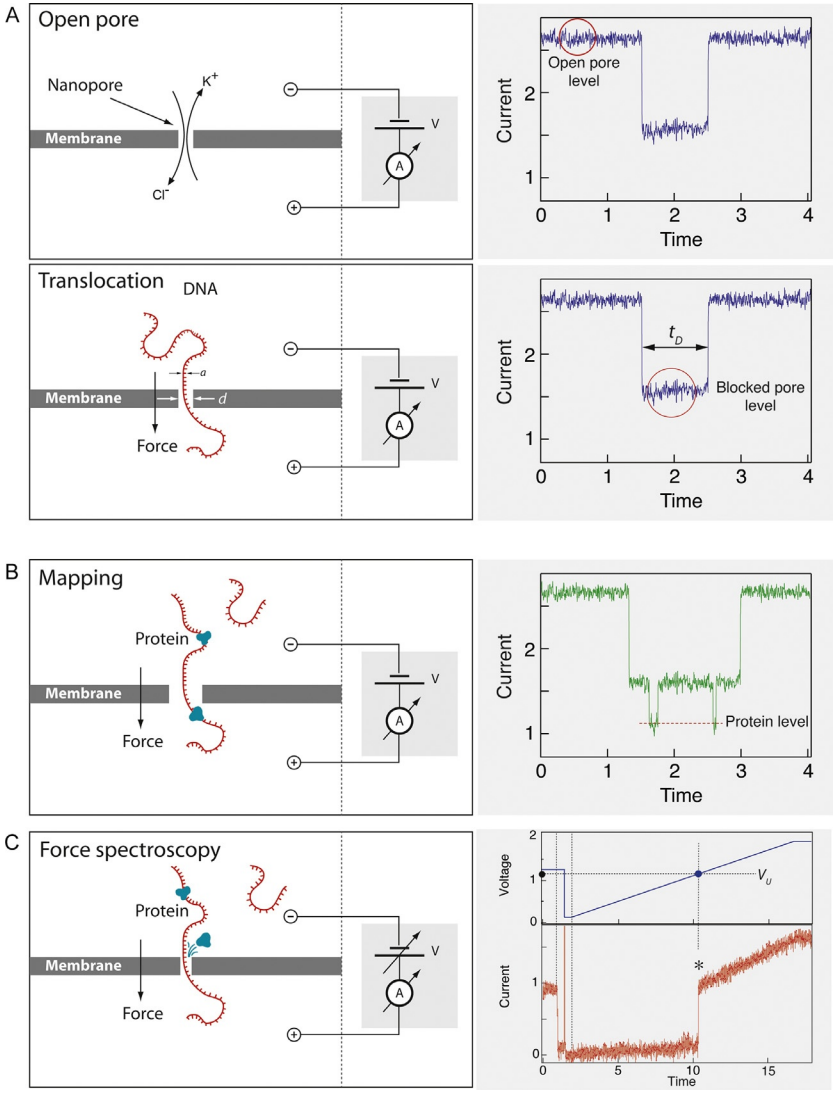


**Fig. 1** Sensing protein–DNA interactions with a nanopore. (A) Translocation of DNA through a nanopore. Voltage is applied across an electrically insulating membrane separating two buffer-filled chambers, drawing ions through the nanopore to create a stable open-pore current. As negatively charged ssDNA is drawn to and through the nanopore, it must uncoil and translocate in a linear end-to-end fashion, blocking the pore and producing a distinctive drop in the ion current as long as it remains in the pore. (B) Method for mapping binding site locations using a nanopore. The nanopore is larger than the protein–DNA complex of interest, and as each complex passes through the nanopore it creates an additional, deeper blockage of the ion current. Because the DNA is scanned linearly as it passes through the nanopore, the positions of these deeper

Bayley, 2013; Talaga & Li, 2009), or enzymatically unfolding the proteins, e.g., by using unfoldase coupled to the nanopore sensors (Nivala, Marks, & Akeson, 2013) and monitoring the changes in the ion current over time as each residue passes through the nanopore. However, protein sequencing is considered to be an even more challenging goal than sm-DNA sequencing, due to the inherent complexity of protein sequence and structure. Perhaps the most challenging aspect of protein sequencing is the identification of the 20 standard amino acids (not to mention the several nonstandard amino acids and various posttranslational modifications) as the unfolded protein is translocated through the nanopore.

The simplicity of the nanopore sensing technique lends itself well to modifications that enable a wide range of additional applications. The development of synthetically fabricated nanopores (often referred to as "solid-state nanopores" or "ssNP") has allowed fine-tuning of nanopore size (diameter and thickness), material properties, and to some extent the morphology of ssNPs, to optimize detection of specific analytes. For example, ssNPs have been crafted for the detection of translocation of native proteins over a wide range of sizes and shapes, from globular ubiquitin (8.5 kDa) to fibrillar amyloid aggregates (Firnkes, Pedone, Knezevic, Döblinger, & Rant, 2010; Fologea, Ledden, McNabb, & Li, 2007; Han et al., 2006; Larkin, Henley, Muthukumar, Rosenstein, & Wanunu, 2014; Nir, Huttner, & Meller, 2015; Plesa et al., 2013; Yusko et al., 2011). The versatility of ssNPs is further extended by treatment of the pore substrate materials with organic or inorganic coatings to alter surface properties (Anderson, Muthukumar, & Meller, 2013; Wanunu & Meller, 2007; Yusko et al., 2011). Recently, several groups have demonstrated the use of exotic materials such as single atomic layers of graphene (Garaj et al., 2010; Merchant et al., 2010; Schneider et al., 2010) or $MoS_2$ (Feng et al., 2015) to create ssNPs, significantly shrinking the length of the sensing region and thereby increasing the pore sensitivity to local analyte structure.

blockages within the current trace roughly correspond to the positions of the protein–DNA complexes. (C) Method for nanopore force spectroscopy. The nanopore is smaller than the protein–DNA complex of interest, so the passage of the DNA is halted when the complex reaches the mouth of the pore. Once the analyte is loaded into position, the electrophoretic force on the DNA is directly modulated by changing the applied voltage, so that eventually the bond between the protein and the DNA will rupture. The time to rupture under various loading schemes can be directly used to infer the binding strength of the protein–DNA complex.

Detection and characterization of nucleic acid–protein interactions, particularly those involving DNA and transcription factors, remain significant barriers to our understanding of genetic regulation. Bound DNA–protein complexes represent local variations in DNA structure that directly affect its function. As nanopores are well suited to investigate the nature of variations in local structure along the length of a molecule (Singer, Rapireddy, Ly, & Meller, 2012; Singer et al., 2010), they provide a natural tool for elucidating the behavior of protein–DNA complexes (Bell & Keyser, 2015; Dorvel et al., 2009; Hall, van Dorp, Lemay, & Dekker, 2009; Hornblower et al., 2007; Kowalczyk, Hall, & Dekker, 2010; Laszlo et al., 2013; Lin, Fabian, Sonenberg, & Meller, 2012; Raillon et al., 2012; Smeets, Kowalczyk, Hall, Dekker, & Dekker, 2009; Soni & Dekker, 2012; Spiering, Getfert, Sischka, Reimann, & Anselmetti, 2011; Squires, Atas, & Meller, 2015; Wallace et al., 2010).

In this review, we focus on development of the nanopore technique for directly sensing DNA/protein complexes. We make a distinction between two principal modes of detection: (i) Mapping: identifying the location of bound proteins along a DNA (or an RNA) biopolymer to reveal where and under what conditions binding occurs. Some typical examples include mapping transcription factors bound to their DNA targets, or sequence-specific localization of peptide nucleic acids to DNA for genotyping applications. (ii) Force spectroscopy: using the nanopore as a tool to disrupt and measure the interaction strength between nucleic acids and bound proteins. This mode of sensing is an exquisite tool for analyzing the binding interactions between nucleic acids and proteins.

## 2. THE BASIC PROPERTIES OF NANOPORE TRANSLOCATION MEASUREMENTS

In a typical nanopore setup, a pair of electrodes is used to apply an electrical potential $\Delta V$ far away (several mm) from a thin insulating membrane separating two chambers and containing the pore (Fig. 1A). The system is filled with a high ionic strength electrolyte solution (physiological conditions or higher). Therefore, even modest electrical potentials (i.e., $\Delta V \sim 0.1$ V) applied across the membrane produce sufficiently large local electrical fields in the pore ($\sim 10^5$ V/cm) to overcome the free energy barrier associated with stretching and threading extremely long, charged biopolymers into the pore (Meller et al., 2001). As a result, molecules such as

DNA and RNA will translocate from the negatively biased *cis* chamber into the *trans* chamber, as shown in Fig. 1A.

As a macromolecule enters the pore, its presence physically excludes a substantial fraction of electrolytes from the pore, causing an abrupt blockade in the ionic current flowing through the pore. Fig. 1A displays schematically the ionic current just before and after the entry/exit of a single DNA molecule into the nanopore. Closer inspection of these current blockades (Fig. 1A, right panel) reveals that the nanopore remains at the blocked level for an extended dwell time ($t_D$). This dwell time has been shown to scale with DNA length, and to grow exponentially with the applied voltage both for protein (Meller et al., 2001) and solid-state nanopores (Wanunu, et al., 2008). Moreover, for solid-state nanopores $t_D$ was also found to decrease exponentially with the pore diameter, $d$ (Wanunu, et al., 2008). Specifically, a small change in pore size (e.g., 1 nm or less) causes a considerable change in dwell time. These findings suggest that $t_D$ represents the passage time (or the "translocation" time) of each biopolymer from *cis* to *trans*. This was further supported by PCR amplification of material from the *trans* chamber (Wanunu, et al., 2008).

The ionic current signal we expect to see due to a DNA–protein complex passing through the nanopore depends entirely on how the complex interacts with the nanopore. If the pore is larger than the complex, the bulky size of the complex relative to bare DNA should create additional blockage of the ionic current, as shown in Fig. 1B. This mode of sensing can be generally classified as nanopore-binding site mapping, and may be used to determine where proteins bind under different conditions. On the other hand, if the pore is not large enough to accommodate the entire protein–DNA complex, the protein will be removed as the DNA passes through the nanopore, as shown in Fig. 1C. This mode of sensing, generally referred to as nanopore force spectroscopy (NFS), probes the strength of the interaction between the protein and the DNA, and/or may be used to investigate the kinetics of a bound enzyme that processively moves DNA through the nanopore.

For nanopore-binding site mapping, the expected signal of interest is a transient blockade below the bare DNA blockade level that marks the passage of the DNA–protein complex, as Fig. 1B (right panel). When the DNA/protein complex passes through the narrowest constriction of the nanopore, its larger size relative to the bare DNA physically excludes more ions from passing through and changes the local electrophoretic ion mobility, causing a corresponding secondary drop in the conductance. At the simplest level, detection of secondary drops in current as shown here can be used

to verify the presence of a protein–DNA complex. On the local scale, this technique can be used to quantify TF-binding affinity for DNA (simply by determining the percent of events observed with binding) under a variety of conditions or for different DNA sequences. Finally, the timing of the secondary blockade(s) relative to the overall translocation of the DNA can be used to determine the position of the protein binding site(s) on the DNA, enabling direct mapping of binding locations.

For NFS, the signal of interest can be related either to the duration of a translocation event relative to the driving voltage, or to the changing ion current after a complex has been halted by the nanopore, as shown in Fig. 1C. A small nanopore is selected in order to permit the passage of DNA, but exclude passage of the bound DNA–protein complex, either forcing removal of bound protein before translocation can resume (signal of interest is duration of translocation) or halt translocation of the complex to observe kinetics (signal of interest is changing ion current after capture). In either case, the presence of the bound complex at the mouth of the pore may cause a secondary blockage of the ion current.

## 3. METHODS FOR NANOPORE FABRICATION AND ASSEMBLY

We describe here the materials and protocols for setting up a sm-experiment using solid-state nanopores. More details regarding setting up nanopore experiments can be found in a previous review (Wanunu & Meller, 2008). Solid-state nanopores are typically fabricated in a thin window of freestanding silicon nitride membrane opened in a silicon chip using standard photolithography methods. 20–50 nm thick low-stress silicon nitride ($SiN_x$) is first deposited on both sides of a silicon wafer using low-pressure chemical vapor deposition. Whole-wafer optical lithography and reactive ion etching (RIE; $SF_6$ etch) are then used to create a hard mask pattern on the back side of the wafer. Free standing $SiN_x$ membranes (typically of size ranging from 10 to 25 μm square) on the front side are created by anisotropic KOH wet etch (Fig. 2A, top panel). In general, smaller windows are desirable due to their superior mechanical stability and lower electrical capacitance (leading to lower overall electrical noise). The $SiN_x$ membrane may be further thinned down to improve the spatial resolution by either creating a locally thinned region using optical lithography and RIE or dry etching the entire wafer using $CF_4$.

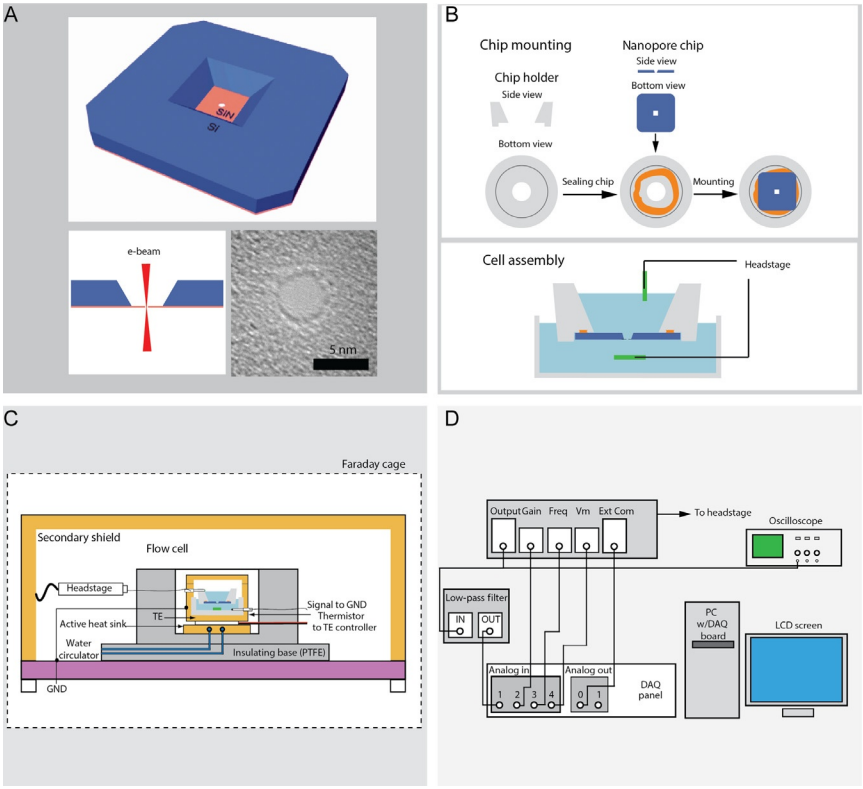


**Fig. 2** Nanopore experimental setup. (A) Solid-state nanopore is fabricated on an ultrathin silicon nitride window supported by a Si chip. The electron beam generated by TEM is tightly focused on the center of the membrane to sputter the materials and create a pore. The TEM micrograph shows typical top view of a drilled pore, obtained right after drilling. (B) Scheme for sealing a nanopore chip onto the chip holder, using a fast curing elastomer. After wetting the pore, the holder is assembled into the cell. (C) The design of a nanopore apparatus optimized for high-bandwidth, low-noise ionic current measurement. The cell is embedded in a matching holder (gold-plated copper) used for thermalization and electromagnetic shielding, surrounded by thermal insulation. The cell can be removed between the measurements for cleaning purpose. This apparatus and the headstage are placed inside a secondary shielding box (copper and aluminum) and a Faraday cage, coupling with a thermoelectric element. (D) Wiring diagram of the basic components needed for ionic current measurement in a nanopore experiment.

The most widely accessible method available for nanopore drilling is direct ablation using a high-resolution, field emission transmission electron microscope (TEM). Briefly, drilling a nanometer scale hole in the ~10–30-nm thick membrane is accomplished by tightly focusing the electron beam on the membrane. Consistent nanopore fabrication was

achieved, for example, using a JEOL 2010F with acceleration voltage of 200 kV and Titan FEI TEM with acceleration voltage of 300 kV at highest magnification (Fig. 2A). At first, only local scarring or thinning of the material will be observed, but a nanoscale hole will develop as more material is removed. TEM tomography reveals an "hour-glass" cross-sectional profile of the drilled pore due to the beam intensity distribution around the central intense point (Kim, Mcnally, Murata, & Meller, 2007). Once formed, the diameter of the nanopore can be tuned by modifying the electron beam intensity and exposure time (Kim, Wanunu, Bell, & Meller, 2006). Alternative solid-state nanopore drilling techniques include focused ion beam lithography, followed by atomic layer deposition to further decrease the pore size (Lo, Aref, & Bezryadin, 2006) or dielectric breakdown (Kwok, Briggs, & Tabard-Cossa, 2014), in which the nanopore is fabricated by the application of high transmembrane potentials leading to the probabilistic production of nanoscale defects in the material which accumulate and ultimately span the membrane.

To perform single-channel recordings using a solid-state nanopore, a sealed electrical cell is assembled such that the chip forms an electrical insulating membrane between two buffer-filled chambers, connected only by the nanopore. Since the nanopore is usually drilled in vacuum, and due to the inherent hydrophobic nature of $SiN_x$ in air, it is important to hydroxylate and clean the nanopore device, especially at the wall inside the nanopore. Untreated hydrophobic pores will not be completely wetted, which may introduce current fluctuations, decrease the open-pore current, or even completely compromise the electrical connection between the two sides of the nanopore. The two main cleaning techniques used for this step are boiling the chip in piranha solution (sulfuric acid and 30% hydrogen peroxide, in 3:1 ratio), and rinsing it with deionized MilliQ water, or alternatively exposing it to oxygen plasma (at the power of 100 W for 1 min).

The treated nanopore chip is then mounted on a custom flow cell housing using either fast-cure silicone polymer as an adhesive or mechanically clamped and sealed using soft O-rings. Both sides of the chip are wetted with the nanopore buffer, and the assembly is placed onto the experimental apparatus (see illustration in Fig. 2B). A typical nanopore buffer is highly conductive buffer solution (e.g., 1 *M* KCl in 20 m*M* Tris or HEPES, pH to desired value). Buffer selection is especially important for studies of protein–DNA interaction, as the buffer must not only be compatible with the nanopore but must also provide the appropriate conditions for binding. Finally, two

Ag/AgCl electrodes complete the circuit, one immersed in the solution of each chamber, connected on their other end to the high-bandwidth amplifier.

The basic principles of building high-bandwidth, low-noise instruments are analogous to the well-established single-channel recording technique. The major consideration is the bandwidth, defined by the low-pass filter. Although high bandwidth provides better time resolution, the root-mean-square noise also increases. Therefore, it is important to select the highest bandwidth that provides a sufficient signal-to-noise ratio. Generally, 10–100 kHz bandwidth is suitable for DNA translocation experiments. The second major consideration is the noise. To minimize low-frequency noise, the apparatus, amplifier, and recording computer must be tied to the same ground. The two main high-gain amplifiers used for nanopores experiments are the Axon amplifier (with maximum bandwidth of ~100 kHz) and the Chimera Instruments (New York, NY) amplifier (with maximum bandwidth of ~1 MHz). Several layers of electrical shielding (including two Faraday cages), temperature, and mechanical stabilization are necessary for precise and reproducible experimental conditions. Fig. 2C depicts an apparatus design for low-noise measurement.

In order to verify that a drilled chip can be used for nanopore measurements, an I–V curve is generated at the beginning of the experiment. The current is measured as a function of ramped voltage. The linearity between current and voltage in both negative and positive bias should be tested. Finally, the pore's conductance is used to calculate the diameter of the nanopore based on the simplified expression:

$$G_{\text{open}} = \sigma \left[ \frac{4l}{\pi d^2} + \frac{1}{d} \right]^{-1}$$

where $G_{\text{open}}$ is the conductivity during the open pore state, $\sigma$ is the bulk conductivity, $d$ is the diameter of the pore, and $l$ is the thickness of the membrane.

For translocation recording, there are two main modes of data acquisition: (1) continuous recording, in which the current and voltage are saved continuously to a storage device, and event-driven acquisition, in which the current and voltage recording is triggered by each translocation event (Meller et al., 2001). An event is defined by a drop in the current below a specific threshold, followed by a rise to the initial current value. An absolute time stamp can be recorded with each event, allowing evaluation of

the event rate in the time domain. (2) In dynamic voltage control mode, an analog trigger is used to generate a predefined voltage pattern, such as a step, a ramp, or any other pattern as the polymer enters the pore. The corresponding current is recorded. Fig. 2D shows a typical wiring diagram of the patch clamp amplifier through a low-pass filter to the DAQ interface panel. The analog output is connected to the external command input of the amplifier for dynamic voltage control.

## 4. NANOPORES FOR MAPPING THE BINDING SITES OF PROTEINS ALONG NUCLEIC ACIDS

Mapping of proteins bound to DNA or RNA should, in principle, be an undertaking comparable to current blockade-based nanopore sequencing approaches. One might even expect that identifying single proteins bound to DNA, which represent relatively large local changes in analyte size, would be easier than detecting the changing blockage levels caused by the passage of different base pairs. In one sense this is correct; DNA–protein complexes differ in diameter from bare DNA by nanometers, on the same order of magnitude as the diameter of bare DNA, while the four nucleobases are of similar chemical structure and composition, and vary in size by mere Ångstroms. However, although gross changes in analyte local structure may be more pronounced for proteins bound to DNA than for variations in DNA sequence, nanopore sensing of protein–DNA binding presents a variety of challenges. Some of these are generally shared with sequencing and other nanopore sensing efforts, e.g., achieving high signal-to-noise ratio or improving spatial and temporal resolution, yet the wide variety of protein–DNA complexes that could be investigated using nanopores demands a much larger engineering parameter space than is necessary for an application with more uniform analytes, such as nucleic acid sequencing.

The primary challenges to mapping protein binding locations along DNA using a nanopore are optimizing temporal and spatial resolution, which in turn depend upon the experimental parameters (pore size and geometry, buffer and voltage selection, etc.) and the resulting signal-to-noise ratio of the ion current blockades. The pore must be large enough to permit passage of the DNA–protein complex, as shown in Fig. 1B, yet small enough to exhibit a clear difference in blockage level or dwell time in the presence of the complex. These parameters vary widely across different protein–DNA complexes of interest. The various challenges in controlling DNA translocation speed have been addressed in detail elsewhere

(Carson & Wanunu, 2015), but in general they may be addressed by any combination of four main approaches: (1) using very small pores, (2) altering the buffer viscosity or ionic species to increase drag on the analyte, (3) inducing an electroosmotic flow countering the translocation direction, and (4) direct control of position using optical tweezers.

Some of the very earliest reports on nanopore translocations pointed out the changes in conductance and translocation time for analytes with different cross-sectional geometry or chemical properties (Wanunu et al., 2009). These observations formed the basis for blockage pattern-based sequencing approaches. Since then, researchers have begun to create synthetic samples with variations in geometry or chemical properties that distinguish or "tag" different regions within a single molecule. Mapping the locations of these tags on analyte molecules is fundamentally similar to mapping of protein–DNA binding sites, with the advantage that covalent or very strongly bound tags circumvent many of the challenges of working with proteins natively bound to DNA.

Mitchell and Howorka engineered a synthetic sample with additional peptide tags to create enhanced local structural variation along a DNA molecule (Mitchell & Howorka, 2008). They modified ssDNA with internal histidine, glycine, arginine, and tyrosine peptide tags, and showed that these bulky groups created characteristic current blockage drops compared to the bare DNA as they translocated through α-hemolysin protein nanopores. Singer and coworkers hybridized peptide nucleic acid (PNA) probes to a long (3500-bp) dsDNA molecule to demonstrate identification of specific short (8-bp) sequences using 4–5 nm diameter solid-state nanopores, as shown in Fig. 3A (Singer et al., 2010). Statistical characterization of the secondary ion current blockades caused by the PNA tags revealed a consistent depth and duration, as observed in the sample event (Fig. 3A, right panel) and indicated that the translocation times of the complexes were ~200× slower (20 μs/bp) than the sections of bare DNA (0.1 μs/bp). This difference was attributed to possible interactions of the complex with the nanopore and/or local kinking of the DNA by the invading PNA tag. This technique was further improved by using γPNA tags to identify genes uniquely from different strains of HIV, which required a careful evaluation of the ability to resolve two neighboring tags (Singer et al., 2012). The shortest resolved distance between neighboring tags was just ~100 bp, and the translocation time between neighboring sites was found to have a power-law dependence on intersite spacing with an exponent of 1.39. Most recently, Plesa et al. designed synthetic DNA constructs with a single-branched

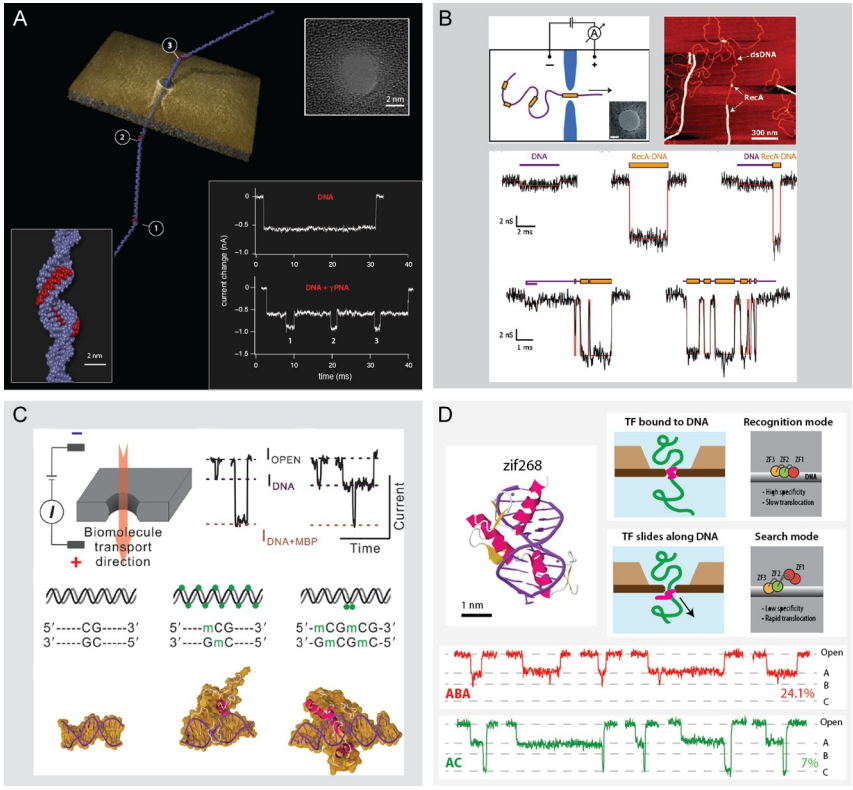


**Fig. 3** Binding site mapping of protein–DNA interactions with solid-state nanopores. (A) Electronic barcoding of a DNA molecule using three sequence-specific γPNA tags. Three distinct secondary blockade levels clearly mark the passage of the PNA tags through a 3.7 nm nanopore. (B) Sensing DNA molecules sparsely coated with RecA protein filaments. *Top left*: schematic of nanopore sensing. *Top right*: AFM image showing patchy RecA coatings on DNA. *Lower*: sample events observed for translocation of these samples through a 30 nm nanopore. Current level changes indicate sensing of distinct DNA and RecA patches. (C) *Top left*: cross-sectional view of nanopore and biomolecule translocation. *Top center*: representative translocation events for bare DNA and hypermethylated DNA bound to MBP1x. *Top right*: representative translocation events for bare DNA and locally methylated DNA bound with a single KzF protein. *Lower*: schematics and crystal structures of DNA and DNA complexed with MBP1x and KzF, respectively. (D) Direct detection of a single small transcription factor, zif268, bound to 1000-bp DNA. *Top left*: crystal structure of bound complex as determined by Elrod-Erickson, Rould, Nekludova, and Pabo (1996). *Bottom*: Sample events observed for translocation of the bound complex through a nanopore are separated into two primary types: shallow blockages during a translocation event (*ABA*), or deep blockages at the end of the event (*AC*). *Top right*: suggested models of transcription factor binding for *ABA* and *AC* events correspond to the known specific and nonspecific binding modes of zif268 (Zandarashvili et al., 2012). *Panel A: Modified with permission from Singer, A.,*

dsDNA marker placed either at the center or near one end of long (7560-bp) dsDNA (Plesa, van Loo, Ketterer, Dietz, & Dekker, 2015). The additional bulk of the 240-bp-long tags created a secondary blockage level as the analyte molecule translocated through ~10 nm diameter pores. Analysis of the temporal positions of these blockages within translocation events indicated that DNA translocation speeds up from beginning to end, with the last 21% of the molecule translocating 19% faster than the first 21% of the molecule. These studies have laid crucial groundwork for analysis of the blockage patterns that are observed for proteins bound to DNA.

Moving closer to detection of native protein–DNA binding sites, Bell and Keyser designed similar synthetic DNA constructs that utilize large proteins (streptavidin and antidigoxigenin) as bulky tags bound with high affinity to small molecules (biotin and digoxigenin, respectively) covalently linked to DNA (Bell & Keyser, 2015). They tagged their 7.2-kbp dsDNA origami carrier molecule with a variety of labeling patterns and demonstrated that as few as one streptavidin per molecule could be identified by the secondary blockage level it created when translocating through 12–18-nm diameter glass capillary nanopores. They were able to resolve easily 3× streptavidin tags spaced ~1800 bp apart, and further demonstrated that these carrier molecules could identify the presence or absence of their specific target protein when preincubated in a mixture of different proteins. One notable drawback to this approach was that 4 *M* LiCl was necessary to reduce DNA translocation velocity through the glass capillary nanopores. These studies of model DNA constructs with designed local tags serve as excellent models to show the expected blockage patterns that can be used to map the locations of proteins bound to DNA, but also highlight the challenges of resolving these and even smaller structures temporally and spatially.

In some cases, detection of protein–nucleic acid interaction via nanopore translocation may be simplified by using a protein that is very large compared to the nucleic acid of interest, or which drastically changes its charge or other

*Rapireddy, S., Ly, D. H., & Meller, A. (2012). Electronic barcoding of a viral gene at the single-molecule level.* Nano Letters, 12*(3), 1722–1728. Panel B: Modified with permission from Kowalczyk, S. W., Hall, A. R., & Dekker, C. (2010). Detection of local protein structures along DNA using solid-state nanopores.* Nano Letters, 10*(1), 324–328. Panel C: Modified with permission from Shim, J., Kim, Y., Humphreys, G. I., Nardulli, A. M., Kosari, F., Vasmatzis, G., et al. (2015). Nanopore-based assay for detection of methylation in double-stranded DNA fragments.* ACS Nano, 9*(1), 290–300. Panel D: Modified with permission from Squires, A., Atas, E., & Meller, A. (2015). Nanopore sensing of individual transcription factors bound to DNA.* Scientific Reports, 5, *1–11.*

characteristics, obviating the need to identify transient secondary blockage levels. These approaches bypass current limits of nanopore resolution through clever assay design, utilizing a large change in the analyte composition to identify the presence of a feature of interest. Carlsen et al. recently demonstrated this principle using a short 90-bp dsDNA oligonucleotide which could be easily distinguished from an otherwise identical internally biotinylated oligonucleotide by incubation with monovalent streptavidin and subsequent evaluation of translocation events through a ~7.5-nm diameter nanopore (Carlsen, Zahid, Ruzicka, Taylor, & Hall, 2014). Translocations of the nonbiotinylated oligo were below the selected temporal resolution of their nanopore assay, but the significant added bulk of streptavidin slowed the translocation of biotinylated samples through the pore so that the detected event rate could be directly used to determine the relative biotinylated:unbiotinylated oligonucleotide ratio in an unknown sample.

At first, it was only possible to detect proteins natively bound to DNA passing through a nanopore if there were many proteins bound to DNA, if the proteins were very large compared to the DNA, or if the position of the DNA could be precisely controlled, e.g., by optical tweezers, to improve the temporal resolution of changing blockage levels due to the passage of a DNA–protein complex. Dekker and coworkers demonstrated the ability to differentiate bare DNA from DNA coated with many large proteins using the DNA-binding protein RecA. RecA is a 37-kDa DNA repair protein which binds nonspecifically along DNA in polymerized clusters to form a helical nucleoprotein filament, stretching the DNA by about 50% and increasing its persistence length to about 950 nm (Hegner, Smith, & Bustamante, 1999). The RecA–DNA complex was estimated to have a local diameter of $7.0 \pm 0.5$ nm (Chen, Yang, & Pavletich, 2008), in contrast to the native 2.2-nm diameter of B-form DNA. Smeets et al. showed that RecA-coated DNA could be easily distinguished from bare DNA using a ~30 nm $SiN_x$ nanopore on the basis of both deeper current blockades and longer translocation times (Smeets et al., 2009). Using optical tweezers in conjunction with ~25 nm $SiN_x$ nanopores, Hall et al. further elucidated the forces on this structure and calculated its effective charge in a nanopore, based on the conductance changes and electrophoretic force measured for RecA–DNA filaments at various ionic strengths (Hall et al., 2009). RecA bound to DNA was also studied in multilayered $Al_2O_3$-graphene nanopores (Venkatesan et al., 2012), and a similar DNA-coating protein, single-stranded binding protein, has been studied in ssNP (Marshall et al., 2015).

Kowalczyk et al. extended the work on RecA by showing that it was possible to detect patterns of protein natively bound to DNA (Kowalczyk et al., 2010). Lowering the concentration of RecA during incubation resulted in incomplete coating of the DNA, forming smaller patches of RecA nucleofilaments which could be distinguished from bare DNA as each type of cross section passed through a ssNP, as shown in Fig. 3B. The sizes and sparsity of these filament patches could be controlled by RecA concentration and binding conditions. However, the speed of translocation and the geometry of the pores used still prevented detection of single RecA molecules bound to DNA.

The first demonstrations of sensing single proteins bound to DNA using a nanopore also required the use of optical tweezers to slow DNA translocation through the nanopore. Sischka et al. employed a similar technique to that described for RecA above to manipulate DNA in the nanopore and measure local force and charge (Sischka et al., 2010). Using optical tweezers to control directly the position of DNA tethered to a trapped beam, they observed discrete, abrupt steps in force during slow dynamic pulling of the DNA through the pore. They attributed these to the translocation of single protein complexes of RecA and also of 2-CysPrx (a peroxiredoxin enzyme which also binds nonspecifically to DNA), as they hopped between two local minimum energy states on either side of the nanopore. Spiering et al. were also able to use optical tweezers to enable nanopore detection of single proteins (EcoRI and RecA) bound to DNA, one of which (EcoRI) binds only at a specific recognition sequence (Spiering et al., 2011).

As nanopore technology has progressed, it has become possible to detect single proteins bound to DNA without the aid of a positioning tool such as optical tweezers. Plesa et al. detected single ~160-kDa antibodies nonspecifically bound to 2.2-kbp DNA using a ~20-nm $SiN_x$ nanopore (Plesa, Ruitenberg, Witteveen, & Dekker, 2015). They observed extremely deep single spikes corresponding to translocation of single anti-DNA antibodies bound to DNA, which was expected given their large excluded volume. The ability to detect single bound proteins greatly extends the range of biologically relevant systems that can be studied with this technique, particularly for proteins whose binding patterns across DNA have implications for gene regulation.

For example, Shim et al. employed a his-tagged single DNA-binding domain of the protein MBD1x to detect methylated DNA by observing deeper and longer current blockages in ~10-nm diameter pores for methylated DNA (36 sites) as compared to unmethylated DNA, to which

MBD1x was exposed in varying ratios (Shim et al., 2013). They found that they could distinguish differences in current and time blockage levels down to a binding ratio of 1:1 MBD1x:DNA (or 1 protein for ~40 binding sites). While they did not observe transitions to secondary ion current blockade levels during these events, they recently were able to detect these for a different methyl-binding protein, Kaiso zinc finger (Kzf), during translocation of 90-bp methylated oligonucleotides (Shim et al., 2015). Fig. 2C shows the structure of MBD1x and Kzf each bound to DNA, and shows sample events for the translocation of bare DNA through the pore as compared to DNA with a single bound protein. For MBD1x, the presence of the protein is evident from the overall depth and duration of the event, while in the case of Kzf, a single spike in the middle of the event shows a secondary blockade level as the protein passes through the pore.

The smallest single proteins bound to DNA detected with a nanopore to date are single zinc finger proteins, as reported in 2015 (Squires et al., 2015; Yu et al., 2015). Fig. 3D shows the structure of zif268 (Elrod-Erickson et al., 1996; Pavletich & Pabo, 1991), the ~10-kDa DNA-binding domain of the transcription factor EGR1. Transcription fingers are of particular interest for DNA–protein binding site mapping because both the sequences to which they bind and the combinations in which they bind are essential components of transcription regulation. To detect such small complexes, it was necessary to use small (3.5-nm diameter), thinned (7-nm long) (Wanunu, Dadosh, et al., 2010) solid-state nanopores to slow the DNA and reduce the sensing volume to improve signal-to-noise ratio of the secondary drop in ion current caused by the passage of the complex through the nanopore. Surprisingly, more than one type of secondary drop in ion current was observed for the translocation of the bound complex: Some events exhibited a small secondary drop near the center of the event, consistent with the binding position and size of the zif268. However, others showed a much deeper, longer blockage, which always occurred at the end of the event. This second population was attributed to the transcription factor entering a nonspecifically bound conformation, which can not only slide along DNA, but which has a larger physical size than the specifically bound conformation (Zandarashvili et al., 2012). In this case, it could slide along the DNA to the very end, at which point it might dissociate from the DNA, producing the observed deep drop at the end of translocation events. These results suggest that nanopores might not only be used to map the binding sites of proteins along DNA but also be useful to observe and classify different binding states directly (Squires et al., 2015). Ongoing improvements to

nanopore fabrication and modification will surely continue to expand the detail with which these complexes may be observed, and in doing so will further broaden the scope of biological questions and applications that can be investigated by mapping binding locations using nanopores.

## 5. NANOPORE FORCE SPECTROSCOPY

Single-molecule force spectroscopy techniques such as optical tweezers, magnetic tweezers, and atomic force spectroscopy allow direct probing of intermolecular binding strengths, and are commonly used to study interactions between individual protein molecules and biopolymers such as DNAs or RNAs (Evans, 2001). Most sm-force spectroscopy techniques require direct tethering of the test molecule to solid surfaces, limiting their application to nonnative proteins or nucleic acids which are modified with specially designed chemical linkers. Additionally, tethering biomolecules reduces the overall throughput of most techniques, since the detector must be scanned over each tether location in turn. In contrast, NFS utilizes the native biomolecule charge (just like gel electrophoresis) to draw individual biomolecules from solutions to the pore area, and to apply an electrophoretic force on the molecule (as shown in Fig. 1). Not only it is tether-free, permitting analysis of native, unmodified biomolecules, but it also senses many molecules in quick succession as they are each drawn to and through the nanopore sensor.

The purpose of NFS experiments is to measure a system's response to an applied force. Importantly, the force applied in NFS is proportional to the molecules' effective charge in the sensing region and is applied at the interface between the pore and the molecule itself. Early NFS experiments were performed using the protein pore α-hemolysin (α-HL) (Hornblower et al., 2007; Mathé, Visram, Viasnoff, Rabin, & Meller, 2004). These studies illustrated the versatility and potential of NFS as an analytical sm-tool (Dudko, Mathé, & Meller, 2010; Dudko, Mathé, Szabo, Meller, & Hummer, 2007). The range of possible biomolecular constructs that can be studied using NFS has been vastly expanded with a series of successive improvements in the fabrication of synthetic nanopores, making it possible to tailor the nanopore geometry and chemical properties to any specific biomolecular complex to be tested (Fologea et al., 2005; Gershow & Golovchenko, 2007; Heng et al., 2004; Smeets et al., 2009; Wanunu & Meller, 2008). While NFS studies all share the basic mechanism of arresting translocation of a protein–DNA complex through a nanopore, the parameters of each experimental setup,

including the size and material of the pore, and the magnitude and timing of the applied force, are broadly tunable.

Kasianowicz et al. showed that a biotinylated ssDNA strand bound to streptavidin can be captured in an α-HL nanopore, but cannot translocate because the streptavidin is too large to fit through the lumen of the pore (Kasianowicz, Henrickson, Weetall, & Robertson, 2001). Later, Bates et al. showed that a real-time feedback control system can be used to change the voltage applied on a DNA strand as it translocates through the pore, effectively modulating the force that the molecule experiences inside the pore (Bates, Burns, & Meller, 2003). These studies formed the basis for capture and manipulation of DNA–protein complexes in NFS.

Similar to other sm-force spectroscopy methods, in NFS information about bond strengths is obtained temporally; in these experiments the key measurement is the distribution of time delays between the application of force and bond rupture measured over many single molecules. Alternatively, the applied force can be ramped at a constant rate; in this case the key measurement is the distribution of critical forces at which bonds are ruptured as a function of the force-ramp slope (or "velocity"). Measuring the response of biomolecules such as DNA and RNA to applied force via NFS can reveal information about self-interactions (unzipping of double-stranded molecules, unzipping of hairpins), mechanical properties, structure, biological function, and also interactions with other molecules such as proteins. NFS allows measurements at atomic-level (sub-nm) spatial resolution and piconewton (pN) force sensitivity (Dudko et al., 2010). NFS experiments are relatively simple to perform and analyze because they do not require any chemical modifications, molecular immobilization, or instrumentation beyond a high-gain patch clamp amplifier. Moreover, because the force is applied at the interface between the nanopore and the biomolecules, NFS could be used to sequentially unfold the structure of long biomolecules, recording the forces required to successively rupture multiple bonds along the biomolecule backbone (Dudko et al., 2010). Perhaps most importantly, NFS can be used to sample many single molecules quickly, allowing rapid acquisition of the bond rupture distributions required for complete analysis and model-fitting of each analyte system (Dudko et al., 2010).

To rupture molecular bonds using NFS or remove an attached molecule, an energy barrier must be crossed. This barrier is much larger than the one associated with threading the unstructured biopolymer through the pore (Dudko et al., 2007; Dudko et al., 2010). Dissociation of bonds due to external force (voltage) is a stochastic process, which can be modeled according to

the Kramers theory of diffusively crossing a free energy barrier (Comer, Ho, & Aksimentiev, 2012). Simple bound systems, such as short hairpins or simple DNA–protein interactions, are well modeled by a single energy barrier. The barrier height and bond stability decrease under external force. Measurements of complicated DNA–protein interactions and unzipping of longer hairpins or duplex regions via NFS involves a more complex process that may require a model with several consecutive energy barriers (Dudko et al., 2010).

In NFS, the ionic current is measured constantly as an indicator of the presence or absence of the analyte within the pore. Once a molecule is captured in the pore, it creates a drop in the ionic current, which can be used to trigger a prescribed voltage change applied by a computerized data acquisition system (Fig. 4A and B). This is a particularly useful aspect of NFS; the voltage used to load analyte molecules into the pore does not have to be the same as the probing voltages, enabling short wait times between successive molecules. Once a molecule is loaded into the pore, one of two voltage patterns can be applied: a constant voltage (fixed-force NFS, illustrated for the case of unzipping a DNA hairpin in Fig. 4A) or a linearly increasing voltage ramp (constant force-ramp NFS, illustrated for the case of unzipping a DNA hairpin in Fig. 4B) (Bates et al., 2003; Dudko et al., 2010). In both cases, the voltage eventually causes a rupture of the bond, which is observed as an abrupt increase in the ionic current as the analyte molecule is freed to exit the pore. The voltage and time at which the bond breaks, called the critical voltage, can be measured and used to calculate the strength of the bond. In fixed-force NFS, the voltage lifetime (time to rupture, $t_U$) of the system is measured directly, as shown in Fig. 4A, while in force-ramp NFS it is determined by processing the distribution of the rupture voltages, $V_U$ (directly proportional to the rupture force), which is measured during the experiments (Fig. 4B). The rupture voltage histograms obtained at different voltage-ramp speeds can be converted to determine the voltage dependence of the bond lifetimes measured at constant voltage (Dudko et al., 2007; Dudko et al., 2010).

Although both NFS approaches (force-ramp and fixed-force) measure the rupture time of the bond, there are practical differences between them. Fixed-force NFS is typically performed at small constant forces; therefore, it can be time consuming and sometimes impractical to wait for rupture of strong bonds. The unzipping timescale depends roughly exponentially on the voltage applied. Force-ramp NFS is faster and allows the same regime of bond strengths to be scanned, because in force-ramp NFS the most likely

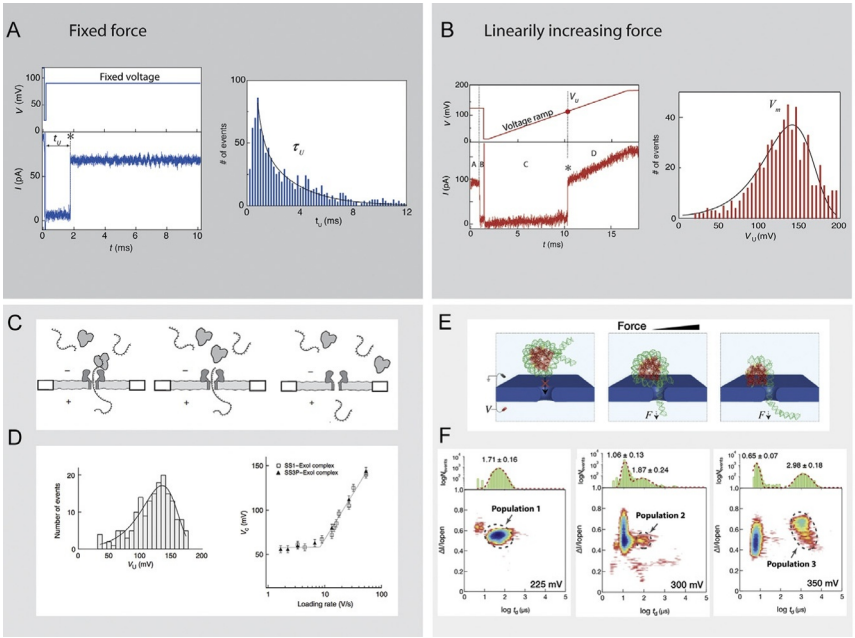


**Fig. 4** Nanopore force spectroscopy. (A and B) The two voltage patterns that are used in NFS experiments: a constant voltage (A) or a linearly increasing voltage (B). In both cases, the capture of the DNA–protein complex results in a decrease in the ionic current and the voltage eventually causes a rupture of the bond, which is detected as an abrupt increase in the current to its original value. In (A), the histogram presents the time at which the bond breaks, $t_u$ measured for each event, and in (B), the histogram presents the rapture voltage, $V_U$ measured for each event. (C) Illustration of DNA–exonuclease NFS experiment: the complex is captured by the pore but cannot translocate. Next, the bond breaks, releasing the bare ssDNA to freely translocate through the pore. (D). *Left side*: histogram presenting the distribution of the voltages at which dissociation of the complex occurs, for a fixed loading rate. The peak of the histogram is defined as the critical voltage $V_C$. *Right side*: the critical voltage vs the loading rate obtained from dynamic NFS experiment of the DNA–Exonuclease complex. At low loading rates, the dissociation voltage is independent of the loading rate, while at higher loading rates there is a logarithmic dependence of the dissociation voltage on the loading rate. (E). Illustration of DNA-histone NFS experiment where ssNP is used to unwind the nucleosome from one end of the DNA. (F). Results from fixed-force NFS experiment of DNA–histone complex: Population 1 representing bare DNA translocations, population 2 representing collisions of the nucleosome complex with the nanopore, and population 3 representing nucleosome unraveling. *Panels A and B: Modified with permission from Dudko, O., Mathé, J., & Meller, A. (2010). Nanopore force spectroscopy tools for analyzing single biomolecular complexes.* Methods in Enzymology, *475, 565–589. Elsevier Inc. Panel C: Modified with permission from Hornblower, B., Coombs, A., Whitaker, R. D., Kolomeisky, A., Picone, S. J., Meller, A., et al. (2007). Single-molecule analysis of DNA-protein complexes using nanopores.* Nature Methods, *4(4), 315–317. Panel D: Modified with permission from Hornblower, B., Coombs, A., Whitaker, R. D., Kolomeisky, A., Picone,*

rupture voltage (the peak in the histogram, $V_m$ in Fig. 4B), has a roughly logarithmic dependence on the voltage ramp speed, enabling sensing of a wider range of unzipping lifetime scales than fixed-force NFS (Mathé, Arinstein, Rabin, & Meller, 2006; Mathé et al., 2004). From these results, the energy barrier between bound and unbound states may be directly calculated.

The sensing region of biological pores typically have small diameters, therefore, these pores are ideal for capturing ssDNA (roughly 1 nm)–protein complexes in the pore and forcing them to dissociate. In addition to their reproducible geometry and chemical profile, these pores are otherwise resilient to a broad range of experimental conditions. For example, the heptameric structure of the α-HL nanopore is stable under high temperatures, voltage gradients (Kang, Cheley, Guan, & Bayley, 2006), and a wide range of ionic strengths (Bonthuis et al., 2006). However, due to the lipid bilayer fragility under high voltage, high loading rates cannot be applied to protein nanopores without compromising the stability of the membranes in which they reside.

NFS was first used by Mathé et al. to unzip DNA hairpins under both fixed and varying forces (Mathe et al., 2006; Mathé et al., 2004). An applied voltage drew analytes to an α-HL pore, where the single-stranded end of each DNA hairpin was captured and extended through the lumen into the stem portion (which has a minimal diameter of roughly 1.4 nm), with the hairpin remaining trapped at the pore's mouth. Crossing the energy barrier to complete translocation required irreversible unzipping of the double-stranded section. Using the distribution of dwell times observed at various applied voltages, they were able to characterize the unzipping energy barrier for each hairpin and study the temperature dependence of the bond-rupturing processes, even resolving single-nucleotide mismatches in the DNA duplexes.

Hornblower and coworkers performed the first demonstration of both fixed-force and force-ramp NFS on protein (Exonuclease 1)–ssDNA

*S. J., Meller, A., et al. (2007). Single-molecule analysis of DNA-protein complexes using nanopores.* Nature Methods, *4(4), 315–317. Panel E: Modified with permission from Ivankin, A., Carson, S., Kinney, S. R. M., & Wanunu, M. (2013). Fast, label-free force spectroscopy of histone–DNA interactions in individual nucleosomes using nanopores.* Journal of the American Chemical Society, 135*(41), 15350–15352. Panel F: Modified with permission from Ivankin, A., Carson, S., Kinney, S. R. M., & Wanunu, M. (2013). Fast, label-free force spectroscopy of histone–DNA interactions in individual nucleosomes using nanopores.* Journal of the American Chemical Society, 135*(41), 15350–15352.*

complexes using a protein nanopore system similar to that used by Mathé et al. (Hornblower et al., 2007) (Fig. 4C). They performed translocation experiments using bare DNA and obtained, as expected, one dominant population in the scatter plot presenting the blockage amplitude vs dwell time for each event. Once the enzyme was added, they observed a second population with longer and broader dwell times. The second population arose due to events in which the DNA–protein complex was captured until it dissociated in the pore, substantially extending the dwell time of the molecules in the pore. After showing that nanopores could be used to dissociate the protein–enzyme bond using a constant voltage (180 mV) they performed dynamic force spectroscopy measurements in order to probe the dissociation kinetics of the complex under voltage ramps. According to their results, the rupture voltage depends on the loading rate (voltage/time). At low loading rates, the dissociation voltage is independent of the loading rate, while at higher loading rates there is a logarithmic dependence of the dissociation voltage on the loading rate (Fig. 4D). These two regimes effectively reflect the Kramers' kinetics of the system. The system attempts to cross the energy barrier at a certain rate, while this barrier height is gradually reduced with the application of the voltage ramp. The kinetic binding constants characterizing the system were calculated using a relatively straightforward theoretical model to fit the data.

While biological pores have been subsequently employed for other NFS studies, e.g., to monitor peptide cleavage by protease and calculate the enzymatic activity of this process (Zhao, de Zoysa, Wang, Jayawardhana, & Guan, 2009), the fixed pore geometry and the limitations on applied forces imposed by bilayer fragility motivated other researchers to begin using synthetic nanopores for NFS. McNally et al. used sub-2 nm solid-state nanopores fabricated in $SiN_x$ membranes to unzip DNA hairpins, showing that single-base mismatches could be resolved in a similar fashion to the biological pores (McNally, Wanunu, & Meller, 2008). Tabard-Cossa et al. demonstrated the advantages of ssNP for higher-force NFS by probing the neutravidin–biotin bond using a 3-nm $SiN_x$ pore (Tabard-Cossa et al., 2009). The biotin was covalently linked to a 94-nucleotide ssDNA molecule which was captured by the pore. The electrostatic force on the DNA in the nanopore was directly transferred to the neutravidin–biotin bond. As expected, the dissociation timescale for this bond was observed to decrease with increasing applied force.

The addition of ssNP to the NFS community quickly precipitated a wide range of other experiments, due to the ease with which ssNP fabrication

could be tailored to the desired application. One such application is to study and measure the binding properties of restriction enzymes to DNA (Dorvel et al., 2009; Zhao et al., 2007). Multiple NFS experiments in which restriction enzymes were removed from DNA by a ssNP showed that there is a voltage threshold for rupture of the enzyme–DNA complex which depends on the enzyme, scales linearly with the dissociation energy, and is highly sensitive to mutations in the recognition sequence. Molecular dynamic simulations of this system are in agreement with these results (Dorvel et al., 2009; Zhao et al., 2007).

More recently, ssNP were used to probe directly the forces between DNA and histones (Ivankin, Carson, Kinney, & Wanunu, 2013; Langecker et al., 2015). Nucleosomes, which consist of a 147-bp dsDNA wrapped around a histone octamer, help packing eukaryotic genomes into the nucleus. DNA packaging also controls crucial biological processes in the cell including transcription, replication, and DNA repair. Large ssNP (~20 nm) had been previously used to detect and distinguish among translocation events of histone monomers, tetramers, histone octamers, mononucleosomes, and dinucleosomes (Soni & Dekker, 2012) based on their charge and size. Ivankin et al. performed NFS on similar samples using smaller pores (~3 nm), which excluded the nucleosome complex while permitting one end of the DNA to enter and be subjected to a pulling force, thereby unwinding the nucleosome from one end of the DNA (Fig. 4E) (Ivankin et al., 2013). By measuring the blockage time and current drop for different applied voltages, they observed that as the voltage increased, two additional classes of ion current blockades were observed (Fig. 4F) that differed from the events observed at low voltage (bare DNA translocations). At about 300 mV, a second population with longer dwell times (in comparison to bare DNA) was observed. However, because the dwell time of these events did not change as the force was increased, this population was attributed to collisions of the nucleosome complex with the nanopore. At 325 mV, they began to detect a third population with much longer translocation times, for which the dwell time decreased with increasing voltage. These events were attributed to nucleosome unraveling (Fig. 4F, right panel). Based on the bare DNA translocation velocities and the critical voltage at which the complex unwinding begins, the strength of the DNA–histone bond could be estimated.

Langecker et al. followed up on this work by performing dynamic force spectroscopy measurements on nucleosome complexes (Langecker et al., 2015). As with previous NFS studies, when a dsDNA tail was captured, signaled by the current dropping beneath a predetermined "trigger" threshold,

the voltage was reduced and ramped upward at a constant loading rate. As a critical voltage was reached, nucleosome rupture (unwinding of the DNA from the histone) began. As expected, the average rupture voltage depended on the loading rate. They further showed that a more stable positioning sequence had higher rupture voltage and longer integrated lifetime, but that DNA methylation did not noticeably alter the rupture voltages. This result suggested a relatively minor impact of methylation on nucleosome packaging and stability, and possibly a greater role for histone modifications.

An entirely separate class of NFS experiments on DNA–protein interactions have employed fixed-force to keep the complex of interest in place while monitoring the activity of an attached enzyme via changing ionic current (Bayley, 2015; Benner et al., 2007; Wanunu, 2012). Benner et al. showed that by introducing the Klenow fragment of *Escherichia coli* DNA polymerase (KF) into the DNA solution, it is possible to slow down the velocity of DNA translocation (Benner et al., 2007). The KF forms a complex with the DNA and a primer in the bulk solution. This complex can enter the nanopore vestibule but is too big to enter the sensing region. Similar to other force spectroscopy measurements, the measured event dwell time directly reports the stability of the complex. Unlike other protein–DNA complexes, the DNA–KF complex is only stable in the presence of $Mg^{2+}$, which is also essential for KF catalytic function. When the correct deoxynucleotide triphosphate (dNTP, complementary to the DNA template) is introduced into the system in the presence of $Mg^{2+}$, the dwell time of the complex in the pore increased by two orders of magnitude compared to the DNA-KF complex in the absence of the correct dNTP and naked DNA. In a follow-up paper, Hurt et al. showed that the dNTP concentration increases the dwell time in unsaturated manner up to 10 m*M* dNTP (Gyarfas et al., 2009; Hurt, Wang, Akeson, & Lieberman, 2009; Lieberman et al., 2010).

Since the initial proof of principle in 2007, DNA polymerase has been widely utilized to position and slow down DNA translocation to achieve significant gains in time resolution. In doing so, it also enables study of DNA polymerase activity with single-base resolution. One of the first applications of nanopore polymerase technology was to detect a single-base change in a DNA strand. Cockroft et al. capped one end of a DNA oligonucleotide with a bulky protein (Cockroft, Chu, Amorin, & Ghadiri, 2008). Once the complex translocated though a small protein pore, a primer was annealed to the other end, trapping the DNA inside the pore. Using TopoTaq DNA polymerase, DNA could then be pulled forward and backward by controlling the transmembrane voltage. This "tug-of-war" strategy

increased the time the DNA resides inside the pore, improving signal-to-noise ratio to the point where a single-base change in a short oligonucleotide could be identified using a residual current histogram. However, this method could not resolve the location of the base change due to inadequate spatial and time resolution (Laszlo et al., 2013; Schreiber et al., 2013).

NFS is advancing on two main fronts in parallel. Probing the nature of static DNA–protein interactions is surprisingly challenging due to the wide variety of protein–DNA interactions that exist, each of which requires a slightly different optimization of nanopore sensing parameters. Probing enzyme activity with NFS is more technically straightforward, as the goal is simply to keep the (very large) complex lodged in place for as long as possible under low applied force, to allow extended observation of enzyme activity. The converse application of this, which is to use the NFS configuration to watch an enzyme's kinetics for the purpose of reporting on the nature of the substrate, is also gaining interest within the sequencing community (Bayley, 2015; Wanunu, 2012). These important aspects of DNA strand regulation by DNA polymerase and enzyme dynamics probed at extremely high resolution are reviewed in "Subangstrom measurements of enzyme function using a biological nanopore, SPRNT" by Laszlo et al. elsewhere in this volume.

## 6. CONCLUSIONS

Nanopores can be used to probe nucleic acid–protein complexes directly in two distinct modes of detection: binding site mapping (detection of the translocating protein–DNA complex) and force spectroscopy (controlled removal of the protein). Together, these could shed light on nucleic acid–protein binding from many different angles, directly measuring where proteins bind on both local and genomic scales, enabling testing of binding conditions, and characterizing the forces and processes that dictate how they bind. In addition to providing a single platform for experimental observation of nucleic acid–protein complexes, nanopores have the unique sensitivity, flexibility, and adaptability to allow study of label-free, unamplified samples—and the ability to do so on length scales ranging from local binding to genome-wide mapping.

Both nanopore-binding site mapping and NFS have greatly benefitted from the ability to modify nanopore size, shape, and materials. For binding site mapping, detection of single natively bound proteins has only been possible through improving the spatial and temporal resolution of the nanopore

to slow translocation and enhance the signal difference between bare DNA and the bound complex, which is achieved primarily through tuning the pore geometry, applied voltage, and buffer conditions. In NFS, it is essential to optimize the dimensions of the pore and the applied force to suit the complex under study. Studies of DNA–enzyme interactions using NFS originally arose from nanopore modifications made in order to control DNA motion in the pore for other applications (i.e., sequencing), but have themselves proven to be an excellent method for direct observation of DNA–enzyme activity. While to date there have been relatively few studies that utilize the versatility of nanopores to study samples in different buffer conditions, we expect that future work will take advantage of this point as well.

In the broader scientific context, it is somewhat surprising that nanopore sequencing has advanced to commercialization while the (comparatively) larger local changes in analyte structure caused by DNA–protein interactions have not been as extensively studied. Commercial factors and the goal of personalized medicine almost certainly play a large role in this disparity, yet the scientific implications of DNA–protein interactions are as essential to understanding cellular function as DNA sequences (and are arguably less well understood). Nanopores have immense potential as a tool to report on many aspects of protein–DNA interactions simultaneously and at the sm-level, revealing where, under what conditions, and how tightly proteins bind. Existing techniques to study DNA–protein interactions, like electromigration shift assays and more, may report on one or more of these points, but surely none can address so broad a spectrum of questions at the sm-level.

Yet these broad impacts may also embody the challenges to implementation of this technique: In contrast to nanopore sequencing, which requires improvements in temporal and spatial resolution to resolve very subtle differences in local structure along just one type of analyte, studies of DNA–protein interaction require optimization across an incredibly broad range of analytes. We anticipate that studies of protein–DNA interactions will be greatly facilitated by future advances in nanopore fabrication and modification, as these will allow optimization of the technique for an expanding range of nucleic acid–protein analytes.

## ACKNOWLEDGMENTS

Financial support from the Marie Curie People award (GA-2010-277060, EC), from the Israeli Centers of Research Excellence (I-CORE) program (Center #1902/12), from the Israeli Science Foundation (award # 845/11), and BeyondSeq program (H2020-634890) are gratefully acknowledged.

## REFERENCES


Akeson, M., Branton, D., Kasianowicz, J., Brandin, E., & Deamer, D. (1999). Microsecond time-scale discrimination among polycytidylic acid, polyadenylic acid, and polyuridylic acid as homopolymers or as segments within single RNA molecules. *Biophysical Journal*, *77*, 3227–3233.

Anderson, B. N., Muthukumar, M., & Meller, A. (2013). pH tuning of DNA translocation time through organically functionalized nanopores. *ACS Nano*, *7*(2), 1408–1414.

Bates, M., Burns, M., & Meller, A. (2003). Dynamics of DNA molecules in a membrane channel probed by active control techniques. *Biophysical Journal*, *84*(4), 2366–2372.

Bayley, H. (2015). Nanopore sequencing: From imagination to reality. *Clinical Chemistry*, *61*(1), 25–31.

Bell, N. A., & Keyser, U. F. (2015). Specific protein detection using designed DNA carriers and nanopores. *Journal of the American Chemical Society*, *137*(5), 2035–2041.

Benner, S., Chen, R. J., Wilson, N. A., Abu-Shumays, R., Hurt, N., Lieberman, K. R., et al. (2007). Sequence-specific detection of individual DNA polymerase complexes in real time using a nanopore. *Nature Nanotechnology*, *2*(11), 718–724.

Bonthuis, D. J., Zhang, J., Hornblower, B., Mathé, J., Shklovskii, B. I., & Meller, A. (2006). Self-energy-limited ion transport in subnanometer channels. *Physical Review Letters*, *97*(12), 128104.

Branton, D., Deamer, D. W., Marziali, A., Bayley, H., Benner, S. A., Butler, T., et al. (2008). The potential and challenges of nanopore sequencing. *Nature Biotechnology*, *26*(10), 1146–1153.

Carlsen, A. T., Zahid, O. K., Ruzicka, J. A., Taylor, E. W., & Hall, A. R. (2014). Selective detection and quantification of modified DNA with solid-state nanopores. *Nano Letters*, *14*(10), 5488–5492.

Carson, S., & Wanunu, M. (2015). Challenges in DNA motion control and sequence readout using nanopore devices. *Nanotechnology*, *26*(7), 074004.

Chen, Z., Yang, H., & Pavletich, N. P. (2008). Mechanism of homologous recombination from the RecA–ssDNA/dsDNA structures. *Nature*, *453*(7194), 489–494.

Cherf, G. M., Lieberman, K. R., Rashid, H., Lam, C. E., Karplus, K., & Akeson, M. (2012). Automated forward and reverse ratcheting of DNA in a nanopore at 5-A precision. *Nature Biotechnology*, *30*(4), 344–348.

Cockroft, S. L., Chu, J., Amorin, M., & Ghadiri, M. R. (2008). A single-molecule nanopore device detects DNA polymerase activity with single-nucleotide resolution. *Journal of the American Chemical Society*, *130*(3), 818–820.

Comer, J., Ho, A., & Aksimentiev, A. (2012). Toward detection of DNA-bound proteins using solid-state nanopores: Insights from computer simulations. *Electrophoresis*, *33*(23), 3466–3479.

Derrington, I. M., Craig, J. M., Stava, E., Laszlo, A. H., Ross, B. C., Brinkerhoff, H., et al. (2015). Subangstrom single-molecule measurements of motor proteins using a nanopore. *Nature Biotechnology*, *33*(10), 1073–1075.

Dorvel, B., Sigalov, G., Zhao, Q., Comer, J., Dimitrov, V., Mirsaidov, U., et al. (2009). Analyzing the forces binding a restriction endonuclease to DNA using a synthetic nanopore. *Nucleic Acids Research*, *37*(12), 4170–4179.

Dudko, O., Mathé, J., & Meller, A. (2010). Nanopore force spectroscopy tools for analyzing single biomolecular complexes. *Methods in enzymology*, *475*, 565–589. Elsevier Inc.

Dudko, O. K., Mathé, J., Szabo, A., Meller, A., & Hummer, G. (2007). Extracting kinetics from single-molecule force spectroscopy: Nanopore unzipping of DNA hairpins. *Biophysical Journal*, *92*(12), 4188–4195.

Elrod-Erickson, M., Rould, M. A., Nekludova, L., & Pabo, C. O. (1996). Zif268 protein–DNA complex refined at 1.6 Å: A model system for understanding zinc finger–DNA interactions. *Structure*, *4*(10), 1171–1180.

Evans, E. (2001). Probing the relation between force-lifetime and chemistry in single molecule bonds. *Annual Review of Biophysics and Biomolecular Structure*, *30*, 105–128.

Feng, J., Liu, K., Bulushev, R. D., Khlybov, S., Dumcenco, D., Kis, A., et al. (2015). Identification of single nucleotides in MoS2 nanopores. *Nature Nanotechnology*, *10*(12), 1070–1076.

Firnkes, M., Pedone, D., Knezevic, J., Döblinger, M., & Rant, U. (2010). Electrically facilitated translocations of proteins through silicon nitride nanopores: Conjoint and competitive action of diffusion, electrophoresis, and electroosmosis. *Nano Letters*, *10*(6), 2162–2167.

Fologea, D., Gershow, M., Ledden, B., McNabb, D. S., Golovchenko, J. A., & Li, J. (2005). Detecting single stranded DNA with a solid state nanopore. *Nano Letters*, *5*(10), 1905–1909.

Fologea, D., Ledden, B., McNabb, D. S., & Li, J. (2007). Electrical characterization of protein molecules by a solid-state nanopore. *Applied Physics Letters*, *91*(5), 053901.

Garaj, S., Hubbard, W., Reina, A., Kong, J., Branton, D., & Golovchenko, J. A. (2010). Graphene as a subnanometre trans-electrode membrane. *Nature*, *467*(7312), 190–193.

Gershow, M., & Golovchenko, J. A. (2007). Recapturing and trapping single molecules with a solid-state nanopore. *Nature Nanotechnology*, *2*(12), 775–779.

Gyarfas, B., Olasagasti, F., Benner, S., Garalde, D., Lieberman, K. R., & Akeson, M. (2009). Mapping the position of DNA polymerase-bound DNA templates in a nanopore at 5 Å resolution. *ACS Nano*, *3*(6), 1457–1466.

Hall, A. R., van Dorp, S., Lemay, S. G., & Dekker, C. (2009). Electrophoretic force on a protein-coated DNA molecule in a solid-state nanopore. *Nano Letters*, *9*(12), 4441–4445.

Han, A., Schürmann, G., Mondin, G., Bitterli, R. A., Hegelbach, N. G., de Rooij, N. F., et al. (2006). Sensing protein molecules using nanofabricated pores. *Applied Physics Letters*, *88*(9), 093901.

Hegner, M., Smith, S. B., & Bustamante, C. (1999). Polymerization and mechanical properties of single RecA–DNA filaments. *Proceedings of the National Academy of Sciences*, *96*(18), 10109–10114.

Heng, J. B., Ho, C., Kim, T., Timp, R., Aksimentiev, A., Grinkova, Y. V., et al. (2004). Sizing DNA using a nanometer-diameter pore. *Biophysical Journal*, *87*(4), 2905–2911.

Hornblower, B., Coombs, A., Whitaker, R. D., Kolomeisky, A., Picone, S. J., Meller, A., et al. (2007). Single-molecule analysis of DNA-protein complexes using nanopores. *Nature Methods*, *4*(4), 315–317.

Hurt, N., Wang, H., Akeson, M., & Lieberman, K. R. (2009). Specific nucleotide binding and rebinding to individual DNA polymerase complexes captured on a nanopore. *Journal of the American Chemical Society*, *131*(10), 3772–3778.

Ivankin, A., Carson, S., Kinney, S. R. M., & Wanunu, M. (2013). Fast, label-free force spectroscopy of histone–DNA interactions in individual nucleosomes using nanopores. *Journal of the American Chemical Society*, *135*(41), 15350–15352.

Kang, X. F., Cheley, S., Guan, X., & Bayley, H. (2006). Stochastic detection of enantiomers. *Journal of the American Chemical Society*, *128*(33), 10684–10685.

Kasianowicz, J., Brandin, E., Branton, D., & Deamer, D. (1996). Characterization of individual polynucleotide molecules using a membrane channel. *Proceeding of the National Academy of Science*, *93*, 13770–13773.

Kasianowicz, J. J., Henrickson, S. E., Weetall, H. H., & Robertson, B. (2001). Simultaneous multianalyte detection with a nanometer-scale pore. *Analytical Chemistry*, *73*(10), 2268–2272.

Kim, M. J., Mcnally, B., Murata, K., & Meller, A. (2007). Characteristics of solid-state nanometer pores fabricated using a transmission electron microscope. *Nanotechnology*, *18*(20), 205302.

Kim, M. J., Wanunu, M., Bell, D. C., & Meller, A. (2006). Rapid fabrication of uniformly sized nanopores and nanopore arrays for parallel DNA analysis. *Advanced Materials*, *18*(23), 3149–3153.

Kowalczyk, S. W., Hall, A. R., & Dekker, C. (2010). Detection of local protein structures along DNA using solid-state nanopores. *Nano Letters*, *10*(1), 324–328.

Kwok, H., Briggs, K., & Tabard-Cossa, V. (2014). Nanopore fabrication by controlled dielectric breakdown. *PLoS One*, *9*(3), e92880.

Langecker, M., Ivankin, A., Carson, S., Kinney, S. R. M., Simmel, F. C., & Wanunu, M. (2015). Nanopores suggest a negligible influence of CpG methylation on nucleosome packaging and stability. *Nano Letters*, *15*(1), 783–790.

Larkin, J., Henley, R. Y., Muthukumar, M., Rosenstein, J. K., & Wanunu, M. (2014). High-bandwidth protein analysis using solid-state nanopores. *Biophysical Journal*, *106*(3), 696–704.

Laszlo, A. H., Derrington, I. M., Brinkerhoff, H., Langford, K. W., Nova, I. C., Samson, J. M., et al. (2013). Detection and mapping of 5-methylcytosine and 5-hydroxymethylcytosine with nanopore MspA. *Proceedings of the National Academy of Sciences*, *110*(47), 18904–18909.

Lieberman, K. R., Cherf, G. M., Doody, M. J., Olasagasti, F., Kolodji, Y., & Akeson, M. (2010). Processive replication of single DNA molecules in a nanopore catalyzed by phi29 DNA polymerase. *Journal of the American Chemical Society*, *132*(50), 17961–17972.

Lin, J., Fabian, M., Sonenberg, N., & Meller, A. (2012). Nanopore detachment kinetics of poly(a) binding proteins from RNA molecules reveals the critical role of C-terminus interactions. *Biophysical Journal*, *102*(6), 1427–1434.

Lo, C. J., Aref, T., & Bezryadin, A. (2006). Fabrication of symmetric sub-5 nm nanopores using focused ion and electron beams. *Nanotechnology*, *17*(13), 3264.

Manrao, E. A., Derrington, I. M., Laszlo, A. H., Langford, K. W., Hopper, M. K., Gillgren, N., et al. (2012). Reading DNA at single-nucleotide resolution with a mutant MspA nanopore and phi29 DNA polymerase. *Nature Biotechnology*, *30*(4), 349–353.

Marshall, M. M., Ruzicka, J., Zahid, O. K., Henrich, V. C., Taylor, E. W., & Hall, A. R. (2015). Nanopore analysis of single-stranded binding protein interactions with DNA. *Langmuir*, *31*(15), 4582–4588.

Mathé, J., Arinstein, A., Rabin, Y., & Meller, A. (2006). Equilibrium and irreversible unzipping of DNA in a nanopore. *Europhysics Letters*, *73*(1), 128–134.

Mathé, J., Visram, H., Viasnoff, V., Rabin, Y., & Meller, A. (2004). Nanopore unzipping of individual DNA hairpin molecules. *Biophysical Journal*, *87*(5), 3205–3212.

McNally, B., Wanunu, M., & Meller, A. (2008). Electromechanical unzipping of individual DNA molecules using synthetic sub-2 nm pores. *Nano Letters*, *8*(10), 3418–3422.

Meller, A., & Branton, D. (2002). Single molecule measurements of DNA transport through a nanopore. *Electrophoresis*, *23*(16), 2583–2591.

Meller, A., Nivon, L., Brandin, E., Golovchenko, J., & Branton, D. (2000). Rapid nanopore discrimination between single polynucleotide molecules. *Proceedings of the National Academy of Sciences*, *97*(3), 1079–1084.

Meller, A., Nivon, L., & Branton, D. (2001). Voltage-driven DNA translocations through a nanopore. *Physical Review Letters*, *86*(15), 3435–3438.

Merchant, C. A., Healy, K., Wanunu, M., Ray, V., Peterman, N., Bartel, J., et al. (2010). DNA translocation through graphene nanopores. *Nano Letters*, *10*(8), 2915–2921.

Mitchell, N., & Howorka, S. (2008). Chemical tags facilitate the sensing of individual DNA strands with nanopores. *Angewandte Chemie International Edition*, *47*(30), 5565–5568.

Nir, I., Huttner, D., & Meller, A. (2015). Direct sensing and discrimination among ubiquitin and ubiquitin chains using solid-state nanopores. *Biophysical Journal*, *108*(9), 2340–2349.

Nivala, J., Marks, D. B., & Akeson, M. (2013). Unfoldase-mediated protein translocation through an [alpha]-hemolysin nanopore. *Nature Biotechnology*, *31*(3), 247–250.

Oukhaled, A., Cressiot, B., Bacri, L., Pastoriza-Gallego, M., Betton, J.-M., Bourhis, E., et al. (2011). Dynamics of completely unfolded and native proteins through solid-state nanopores as a function of electric driving force. *ACS Nano*, *5*(5), 3628–3638.

Pastoriza-Gallego, M., Rabah, L., Gibrat, G., Thiebot, B., van der Goot, F. G., Auvray, L., et al. (2011). Dynamics of unfolded protein transport through an aerolysin pore. *Journal of the American Chemical Society*, *133*(9), 2923–2931.

Pavletich, N. P., & Pabo, C. O. (1991). Zinc finger-DNA recognition: Crystal structure of a Zif268-DNA complex at 2.1 A. *Science*, *252*(5007), 809–817.

Payet, L., Martinho, M., Pastoriza-Gallego, M., Betton, J.-M., Auvray, L., Pelta, J., et al. (2012). Thermal unfolding of proteins probed at the single molecule level using nanopores. *Analytical Chemistry*, *84*(9), 4071–4076.

Plesa, C., Kowalczyk, S. W., Zinsmeester, R., Grosberg, A. Y., Rabin, Y., & Dekker, C. (2013). Fast translocation of proteins through solid state nanopores. *Nano Letters*, *13*(2), 658–663.

Plesa, C., Ruitenberg, J. W., Witteveen, M. J., & Dekker, C. (2015). Detection of individual proteins bound along DNA using solid-state nanopores. *Nano Letters*, *15*(5), 3153–3158.

Plesa, C., van Loo, N., Ketterer, P., Dietz, H., & Dekker, C. (2015). Velocity of DNA during translocation through a solid state nanopore. *Nano Letters*, *15*(1), 732–737.

Raillon, C., Cousin, P., Traversi, F., Garcia-Cordero, E., Hernandez, N., & Radenovic, A. (2012). Nanopore detection of single molecule RNAP–DNA transcription complex. *Nano Letters*, *12*(3), 1157–1164.

Rodriguez-Larrea, D., & Bayley, H. (2013). Multistep protein unfolding during nanopore translocation. *Nature Nanotechnology*, *8*(4), 288–295.

Schneider, G. g. F., Kowalczyk, S. W., Calado, V. E., Pandraud, G. g., Zandbergen, H. W., Vandersypen, L. M. K., et al. (2010). DNA translocation through graphene nanopores. *Nano Letters*, *10*(8), 3163–3167.

Schreiber, J., Wescoe, Z. L., Abu-Shumays, R., Vivian, J. T., Baatar, B., Karplus, K., et al. (2013). Error rates for nanopore discrimination among cytosine, methylcytosine, and hydroxymethylcytosine along individual DNA strands. *Proceedings of the National Academy of Sciences*, *110*(47), 18910–18915.

Shim, J., Humphreys, G. I., Venkatesan, B. M., Munz, J. M., Zou, X., Sathe, C., et al. (2013). Detection and quantification of methylation in DNA using solid-state nanopores. *Scientific Reports*, *3*, 1389.

Shim, J., Kim, Y., Humphreys, G. I., Nardulli, A. M., Kosari, F., Vasmatzis, G., et al. (2015). Nanopore-based assay for detection of methylation in double-stranded DNA fragments. *ACS Nano*, *9*(1), 290–300.

Singer, A., Rapireddy, S., Ly, D. H., & Meller, A. (2012). Electronic barcoding of a viral gene at the single-molecule level. *Nano Letters*, *12*(3), 1722–1728.

Singer, A., Wanunu, M., Morrison, W., Kuhn, H., Frank-Kamenetskii, M., & Meller, A. (2010). Nanopore based sequence specific detection of duplex DNA for genomic profiling. *Nano Letters*, *10*(2), 738–742.

Sischka, A., Spiering, A., Khaksar, M., Laxa, M., Konig, J., Dietz, K. J., et al. (2010). Dynamic translocation of ligand-complexed DNA through solid-state nanopores with optical tweezers. *Journal of Physics: Condensed Matter*, *22*(45), 454121.

Smeets, R. M. M., Kowalczyk, S. W., Hall, A. R., Dekker, N. H., & Dekker, C. (2009). Translocation of RecA-coated double-stranded DNA through solid-state nanopores. *Nano Letters*, *9*(9), 3089–3095.

Soni, G. V., & Dekker, C. (2012). Detection of nucleosomal substructures using solid-state nanopores. *Nano Letters*, *12*(6), 3180–3186.

Spiering, A., Getfert, S., Sischka, A., Reimann, P., & Anselmetti, D. (2011). Nanopore translocation dynamics of a single DNA-bound protein. *Nano Letters*, *11*(7), 2978–2982.

Squires, A., Atas, E., & Meller, A. (2015). Nanopore sensing of individual transcription factors bound to DNA. *Scientific Reports*, *5*, 1–11.

Tabard-Cossa, V., Wiggin, M., Trivedi, D., Jetha, N. N., Dwyer, J. R., & Marziali, A. (2009). Single-molecule bonds characterized by solid-state nanopore force spectroscopy. *ACS Nano*, *3*(10), 3009–3014.

Talaga, D. S., & Li, J. (2009). Single-molecule protein unfolding in solid state nanopores. *Journal of the American Chemical Society*, *131*(26), 9287–9297.

Venkatesan, B. M., Estrada, D., Banerjee, S., Jin, X., Dorgan, V. E., Bae, M.-H., et al. (2012). Stacked graphene-Al2O3 nanopore sensors for sensitive detection of DNA and DNA–protein complexes. *ACS Nano*, *6*(1), 441–450.

Wallace, E. V. B., Stoddart, D., Heron, A. J., Mikhailova, E., Maglia, G., Donohoe, T. J., et al. (2010). Identification of epigenetic DNA modifications with a protein nanopore. *Chemical Communications*, *46*(43), 8195–8197.

Wanunu, M. (2012). Nanopores: A journey towards DNA sequencing. *Physics of Life Reviews*, *9*(2), 125–158.

Wanunu, M., Dadosh, T., Ray, V., Jin, J., McReynolds, L., & Drndic, M. (2010). Rapid electronic detection of probe-specific microRNAs using thin nanopore sensors. *Nature Nanotechnology*, *5*(11), 807–814.

Wanunu, M., & Meller, A. (2007). Chemically modified solid-state nanopores. *Nano Letters*, *7*(6), 1580–1585.

Wanunu, M., & Meller, A. (2008). Single-molecule analysis of nucleic acids and DNA–protein interactions using nanopores. In T. Ha & P. Selvin (Eds.), *Laboratory manual on single molecules*: Cold Spring Harbor Press, Cold Spring Harbor, NY. 507.

Wanunu, M., Morrison, W., Rabin, Y., Grosberg, A. Y., & Meller, A. (2010). Electrostatic focusing of unlabelled DNA into nanoscale pores using a salt gradient. *Nature Nanotechnology*, *5*(2), 160–165.

Wanunu, M., Sutin, J., McNally, B., Chow, A., & Meller, A. (2008). DNA translocation governed by interactions with solid-state nanopores. *Biophysical Journal*, *95*(10), 4716–4725.

Wanunu, M., Sutin, J., & Meller, A. (2009). DNA profiling using solid-state nanopores: Detection of DNA-binding molecules. *Nano Letters*, *9*(10), 3498–3502.

Yu, J.-S., Lim, M.-C., Huynh, D. T. N., Kim, H.-J., Kim, H.-M., Kim, Y.-R., et al. (2015). Identifying the location of a single protein along the DNA strand using solid-state nanopores. *ACS Nano*, *9*(5), 5289–5298.

Yusko, E. C., Johnson, J. M., Majd, S., Prangkio, P., Rollings, R. C., Li, J., et al. (2011). Controlling protein translocation through nanopores with bio-inspired fluid walls. *Nature Nanotechnology*, *6*(4), 253–260.

Zandarashvili, L., Vuzman, D., Esadze, A., Takayama, Y., Sahu, D., Levy, Y., et al. (2012). Asymmetrical roles of zinc fingers in dynamic DNA-scanning process by the inducible transcription factor Egr-1. *Proceedings of the National Academy of Sciences*, *109*(26), E1724–E1732.

Zhao, Q., de Zoysa, R. S., Wang, D., Jayawardhana, D. A., & Guan, X. (2009). Real-time monitoring of peptide cleavage using a nanopore probe. *Journal of the American Chemical Society*, *131*(18), 6324–6325.

Zhao, Q., Sigalov, G., Dimitrov, V., Dorvel, B., Mirsaidov, U., Sligar, S., et al. (2007). Detecting SNPs using a synthetic nanopore. *Nano Letters*, 7(6), 1680–1685.